Geochemical Perspectives Letters

Activity coefficients of siderophile elements in Fe-Si liquids at high pressure

K. Righter, R. Rowland, II, S. Yang, M. Humayun

Supplementary Information

The Supplementary Information includes:

- 1) Experimental and Analytical Techniques
- 2) Phase Equilibria and Equilibrium
- 3) Determination of Epsilon Interaction Parameters
- 4) Stability of Phosphides in Early Earth Mantle
- Figures S-1 to S-3
- Supplementary Information References

1) Experimental and Analytical Techniques

Starting materials were a mixture of natural Knippa basalt (Lewis *et al*., 1993) (70% by mass), Fe metal (25% by mass), and Au metal (5% by mass); this is the same mixture as those used in previous studies at 1 GPa (Righter *et al*., 2018). Gold has a very low solubility in silicate melts and if natural (ppm) levels in the metal were used, it would be undetectable in the silicate melt. Therefore, Au was added to these higher levels to make its concentrations higher and detectable in the silicate melts. We know from our previous studies that addition of ~5% Au makes the solubility levels high enough to be measured in the quenched silicate melts of the run products (*e.g.*, Righter *et al*., 2015, 2018).

Finally, silicon metal was added to the silicate and metal mixtures at increments of 2 wt% (2, 4, 6, 8, and 10% by weight), to ensure a wide range of Si alloyed in the final quenched metallic liquids.

Experiments were carried out using the 880-ton multi-anvil press in the Experimental Petrology Laboratory, in the Astromaterials Research and Exploration Science Division at NASA Johnson Space Center. To attain PT conditions of 10 GPa and 2373 K, we utilised a 10/5 assembly (available through COMPRES; Leinenweber *et al*., 2012) in a Walker-module (Walker *et al*., 1990). Pressure was calibrated for this assembly using three different transitions between 9 and 20 GPa: SiO_2 transitions at 9.4 GPa and 1873 K), the transition in $(Mg_{82}Fe_{18})_2SiO_4$ from olivine to wadsleyite at 13.4 GPa and 1673 K, and the transition in Mg_2SiO_4 from wadsleyite to ringwoodite at 20.0 GPa and 1873 K. The assembly utilises a pre-cast ceramic octahedral pressure medium, Re foil furnaces, pyrophyllite gaskets, and temperature is monitored with type C Re/W thermocouples (Righter *et al*., 2008). Uncertainty in temperature and pressure are ±15-20 K and ±0.5 GPa, respectively, based on temperature gradients no larger than 25 K; the emf of the thermocouple has not been pressure-corrected. Single crystal MgO capsules contained the metal and silicate mixtures, and once loaded into the assembly, were pressurised before heating to the run temperature. Thermocouple failure in some cases led to the need to heat by power curve which was established using the correlation between power and temperature from previous experiments. Experimental run durations at the desired temperature were between 1 and 5 min, required to approach equilibrium; shutting off power to the experiments ensured a rapid temperature drop and quenching of the run products.

Metals and quenched silicate glasses were analysed for major and minor elements with Electron Probe Microanalysis (EPMA) at NASA Johnson Space Center using a Cameca SX100 microprobe. Operating conditions for metals and silicates included 15 kV accelerating voltage and 30 nA sample current, and 15 kV accelerating voltage and 20 nA sample current, respectively. In addition, standardisation was done using various metal (Fe, Ni metal), glass (basalt), and mineral (diopside, rhodonite, rutile, potassium feldspar, apatite, olivine) standards. Some metals and glasses had coarse-grained quench texture, and thus a defocused electron beam of 20-30 μm diameter was used for analysis. In these cases, 30-50 analytical points were averaged to obtain a representative composition. Uncertainties in microprobe analyses are ~1% for Ti, Fe, Mn, Ca, and K, and 2% for Si, Al, Mg, Na, and P.

Some elements were present in quantities too low to be detectable using EMPA. Therefore, many trace elements (defined as being <100 ppm in concentration) were measured using a more sensitive analytical approach -

Laser Ablation Inductively Coupled Plasma Mass Spectrometry (LA-ICP-MS). Each sample was analysed by an ElectroScientific Instruments (ESI) New Wave™ UP193FX excimer (193 nm) laser ablation system coupled to a Thermo Element XR™ Inductively Coupled Plasma Mass Spectrometer (ICP-MS) at the Plasma Analytical Facility of the National High Magnetic Field Laboratory, Florida State University. Isotopes measured included ^{29}Si, ^{31}P, ^{51}V, ^{53}Cr, ^{55}Mn, ^{57}Fe, ^{66}Zn, ^{71}Ga, ^{93}Nb, ^{111}Cd, ^{120}Sn, ^{182}W, ^{197}Au, ^{208}Pb, following the analytical protocol of Yang *et al*. (2015). ^{57}Fe and ^{29}Si were used as internal standards for metal+sulfide and for silicates, respectively. Laser fluence was 2 GW/cm^2, and relevant isobaric interferences are discussed in Yang *et al*. (2015). Relative sensitivity factors were obtained using Hoba IVB (Walker *et al*., 2008), Filomena IIA (Wasson *et al*., 1989) and NIST SRM 1263a for siderophile elements (Humayun *et al*., 2007; Gaboardi and Humayun, 2009; Humayun, 2012) and NIST SRM 610 glass, USGS basaltic glasses BHVO-2G, BIR-1G, and BCR-2G for lithophile elements (Jochum *et al*., 2011). Spot sizes of 50 μm at 50 Hz for 10 seconds were used to measure both silicate and metal portions of the samples. The average of multiple analyses (2-5) was used to obtain the representative compositions for silicates and metals in each sample. In all samples, Au, P, V, Mn, Ga, Zn, Cd, Sn, W, Pb, and Nb were detectable in both metals and silicates and thus all 11 elements could be included in the investigation. The relative standard deviation (RSD) of ~5% is typical for elemental abundances in metal and silicate from each of the runs.

2) Phase Equilibria and Equilibrium

In all experiments, metallic liquid equilibrated with silicate melt, and the MgO capsule reacted with the silicate melt to form more MgO-rich liquids. The run products contain a mixture of glass and coarse-grained, skeletal-shaped, quench silicate crystals (Figure 1), because most of our liquids contain > 20% MgO, and MgO-rich silicate melts are generally difficult to quench to a glass even at high quench rates. Similarly, metallic liquids also quench to a matte of quench crystals, rather than a single phase. For analyses of our run products, metallic regions were selected from the largest metallic spheres, and closest to the silicate melt regions. Typically several large (50 μm) spots were measured on any given metallic sphere and then averaged to obtain a representative analysis. For silicate melts analyses, multiple 50 μm spots were identified and selected that were representative of the melt, and avoiding capsule MgO, small metallic blebs, or equilibrium growth oxides or silicates that might interfere with determination of a liquid composition. This approach has been discussed and reported in detail by (Righter *et al*., 2017).

Some studies of HSEs report the stability and existence of micronuggets of HSE-rich metal (*e.g.*, Ertel *et al*., 2008; Malavergne *et al*., 2016), and because Au is an HSE, and we have added a small amount of Au (5%) to the metallic portion of the experiment, this effect must be considered. However, we observed no HSE or Au micronuggets in our experiments (Fig. 1). Furthermore, if any HSE particles appeared as "spikes" in the analysis of the glasses, they could be filtered out during the data reduction, as also explained by (Righter *et al*., 2015).

In order to promote more reduced conditions in the experiments, elemental Si was added to the metal phase. Oxygen fugacity can be calculated relative to the iron-wüstite (IW) oxygen buffer, and we used the expression $\Delta IW = -2*\log [X_{Fe}/X_{FeO}]$, or otherwise referred to as "ΔIW". The ΔIW values for our experiments ranged from ~ -3.3 for low Si runs to ~ -6.4 for Si bearing runs (Table 1). ΔIW can also be calculated using activities of Fe and FeO instead of mole fractions, and thus the equation becomes $\Delta IW = -2*\log [a_{Fe}/a_{FeO}]$. For this calculation a_{Fe} in metal was calculated using the epsilon interaction parameter model for metallic liquids (*e.g.*, Righter *et al*., 2018), and a_{FeO} in silicate melt was calculated using the results of Holzheid *et al*. (1997). ΔIW values calculated using activities are slightly higher than those using mole fractions, from IW-2.9 to -6.11 (Table 1). Most studies utilise the mole fraction approach, and therefore we include those in the tables and figures. However, it is important to understand the difference in these two approaches that is caused by the non-ideality in the Fe-Si system. Activities are used in all the calculations of accretion and core-mantle equilibrium. The range of ΔIW values typically considered relevant to Earth's accretion and core formation is IW-4 to IW-2, and falling right in the middle of the range of relative fO_2 for these experiments. This relative fO_2 brack*et al*so produces a wide range of Si concentrations in the metal (and thus of ln $(1-X_{Si})$) that minimises error on the epsilon value.

3) Determination of Epsilon Interaction Parameters

Concentrations of Au, P, and other siderophile elements in metal and silicate (see Supplementary Information sections 1 and 2) were used to calculate Fe-M exchange K_d according to this equation (where M is the trace element of interest):

$$MO_{(n/2)}^{sil} + (n/2)Fe^{met} = M^{met} + (n/2)FeO^{sil} \quad \text{(Eq. S-1)}$$

Equation S-1 can be expanded to,

$$\ln K = \ln \frac{[a_M^{metal}][a_{FeO}^{silicate}]^{n/2}}{[a_{MO(n/2)}^{silicate}][a_{Fe}^{metal}]^{n/2}} = \ln \frac{[X_M^{metal}][X_{FeO}^{silicate}]^{n/2}}{[X_{MO(n/2)}^{silicate}][X_{Fe}^{metal}]^{n/2}} + \ln \frac{[\gamma_M^{metal}][\gamma_{FeO}^{silicate}]^{n/2}}{[\gamma_{MO(n/2)}^{silicate}][\gamma_{Fe}^{metal}]^{n/2}} \quad \text{(Eq. S-2)}$$

Then, setting $K_d = \frac{[X_M^{metal}][X_{FeO}^{silicate}]^{n/2}}{[X_{MO(n/2)}^{silicate}][X_{Fe}^{metal}]^{n/2}}$ and using the approach detailed by Wood *et al*., (2014), the ratio of oxide activity coefficients in the silicate, $\frac{[\gamma_{FeO}^{silicate}]^{n/2}}{[\gamma_{MO(n/2)}^{silicate}]}$, is assumed to be constant because the silicate melt compositions in this study are all similar. The metal composition, however, varies significantly in Si content and the ratio of activity coefficients in the metal, $\frac{[\gamma_M^{metal}]}{[\gamma_{Fe}^{metal}]^{n/2}}$, is dependent upon variation in metal composition. The above equations are re-arranged yielding:

$$\ln K_d = \text{constant} + n/2 \ln \gamma_{Fe}^{metal} - \ln \gamma_M^{metal} \quad \text{(Eq. S-3)}$$

Equation S-3 is then combined with $\ln \gamma_M^{metal} = \ln \gamma_{Fe}^{metal} + \ln \gamma_M^0 - \varepsilon_M^{Si} \ln(1-X_{Si})$ to become:

$$\ln K_d - (n/2 - 1) \ln \gamma_{Fe}^{metal} = \text{const} - \ln \gamma_M^0 + \varepsilon_M^{Si} \ln(1-X_{Si}) \quad \text{(Eq. S-4)}$$

In Equation S-4, γ_M^0 is defined as the activity coefficient of M at infinite dilution, γ_{Fe}^{metal} is defined as the activity coefficient of Fe in Fe metal (*e.g.*, as in Righter *et al*., 2017, 2018), and ε_M^{Si} is an interaction parameter (*e.g.*, Lupis, 1983) that is a measure of the effect of a solute such as Si (in Fe metallic liquid) on the activity of a trace element that liquid (*e.g.*, As, Sb, Ge, or In; Righter *et al*., 2017). The slope of $\ln K_d$ versus $\ln(1-X_{Si})$ in Equation S-4 provides ε_M^{Si} directly for each element at 2373 K and 10 GPa.

The interaction parameter ε_M^{Si} can be used to calculate activity coefficients (γ) for a trace metal (i) in a multi-component (N) system according to:

$$\begin{aligned} \ln \gamma_i = {} & \ln \gamma_{Fe} + \ln \gamma_i^0 - \varepsilon_i^j \ln(1 - X_i) \\ & - \sum_{j=1(j\neq i)}^{N-1} \varepsilon_i^j X_j \left(1 + \frac{\ln(1 - X_j)}{X_j} - \frac{1}{1 - X}\right) \\ & + \sum_{j=1(j\neq i)}^{N-1} \varepsilon_i^j X_j^2 X_i \left(\frac{1}{1 - X_i} + \frac{1}{1 - X_j} + \frac{X_i}{2(1 - X_i)^2} - 1\right) \end{aligned}$$

Where X_i, X_j and γ_i, γ_j are mole fractions and activity coefficients of components i and j, respectively, and γ_i^0 is the activity of i in Fe at infinite dilution (from Ma, 2001; Righter *et al*., 2017). We calculated interaction parameter ε_M^{Si} for Au, P, V, Mn, Ga, Zn, Cd, Sn, W, Pb, and Nb, by using a linear fit to the data, with the standard error (1 sigma) and the fits passing variance tests in SigmaPlot 12.0.

4) Stability of Phosphides in Early Earth Mantle

Phosphorus can be stable in phosphates and phosphides, with the latter being more soluble than the former. Some have argued that phosphates are stable to secondary alteration processes in the crust, thus locking up P and requiring an extraterrestrial late accreted source (Pasek, 2008). However, P prefers more soluble phosphides at early terrestrial mantle oxygen fugacities of IW-2, based on the equilibrium:

$$2P + 3CaSiO_3 + 5/2O_2 = Ca_3(PO4)_2 + 3SiO_2 \quad \text{(Eq. S-5)}$$

and thermodynamic data from Robie *et al*. (1978) (Fig. S-3). Phosphides may thus facilitate transfer of P to the crust by secondary alteration processes in the early Earth.

Supplementary Figures

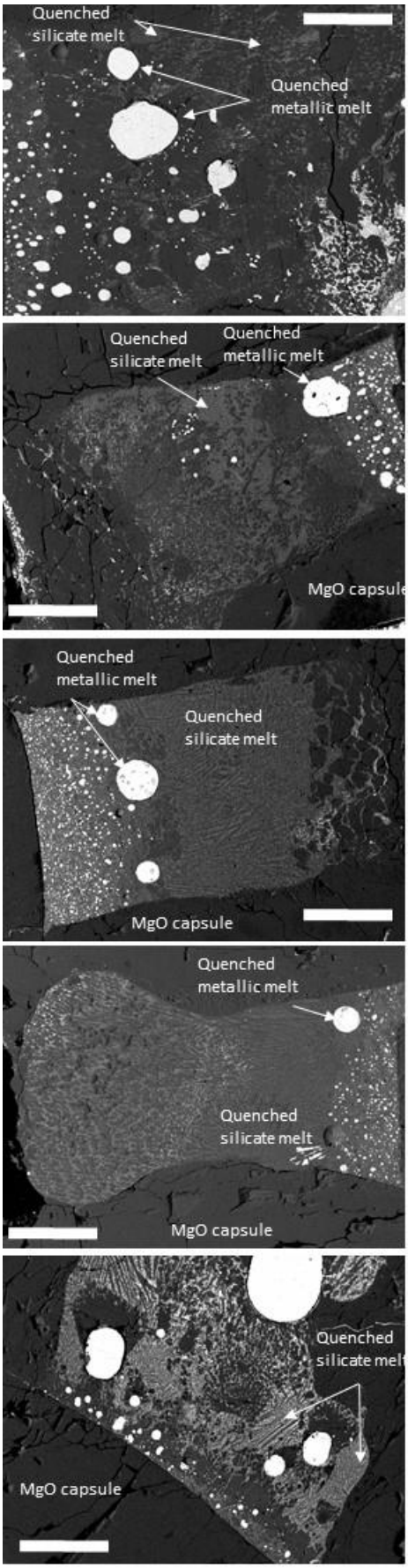

Figure S-1 BSE images of Experiments 2, 3, 5, 6, and 7. For each experiment, images show the bright white metallic liquid, and lighter gray silicate melts which mostly quenched to a matte of quench crystals. All experiments were carried out in MgO capsules, which reacted slightly with the silicate melt. All scale bars are 200 μm.

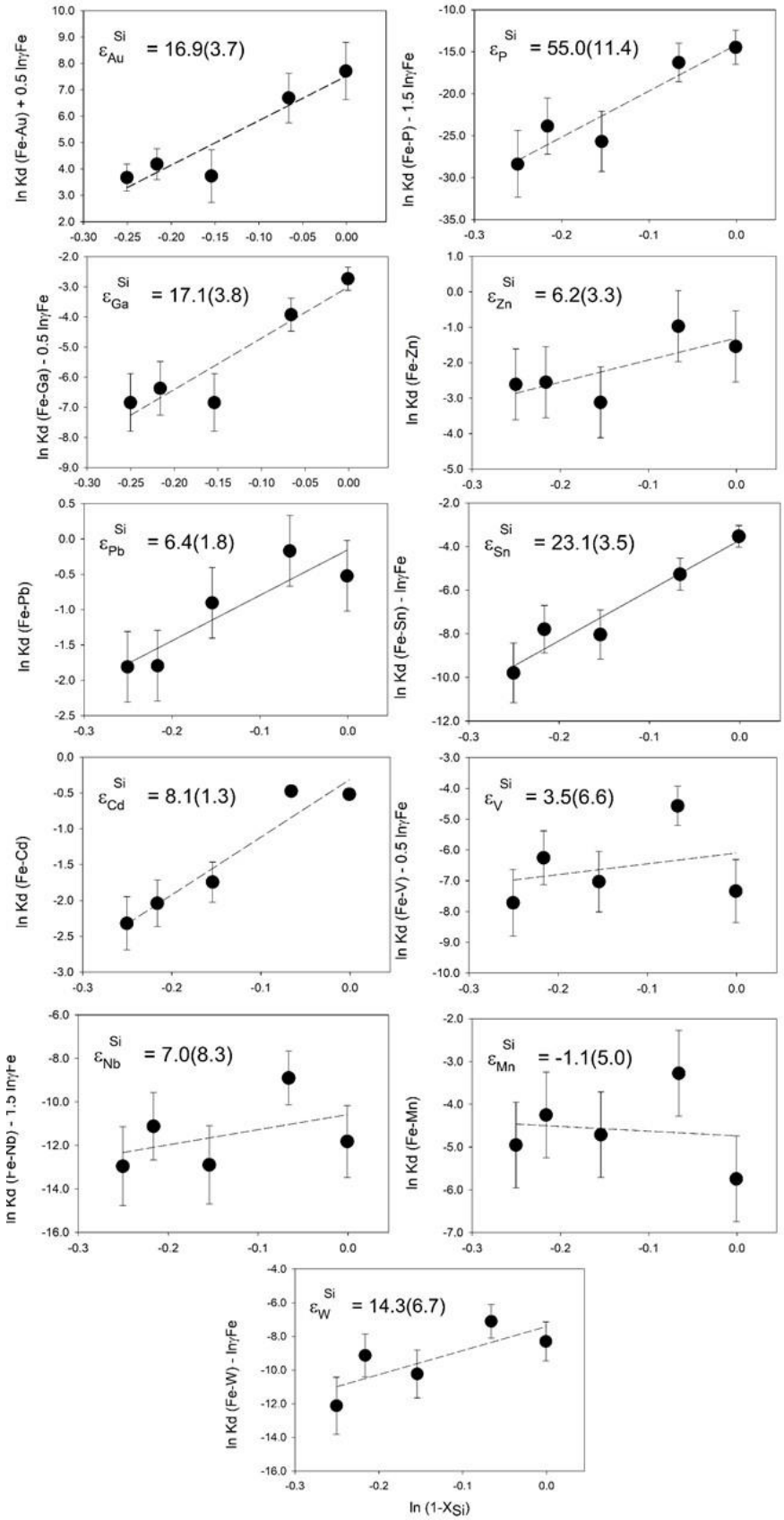

Figure S-2 ln K_d versus ln (1-Xsi) for all elements measured in this study. lnK_d(Fe-X^{5+})–1.5ln(γ_{Fe}), ln K_d(Fe-X^{4+})–ln(γ_{Fe}), ln K_d(Fe-X^{3+})–0.5ln(γ_{Fe}), ln K_d(Fe-X^{2+}), and ln K_d(Fe-X^{1+})+0.5ln(γ_{Fe}) versus ln(1-X_{Si}) from experiments across a wide range of Si contents in metallic Fe. The slope of the lines yields the interaction parameter for each – ε_X, - in Fe-Si liquids.

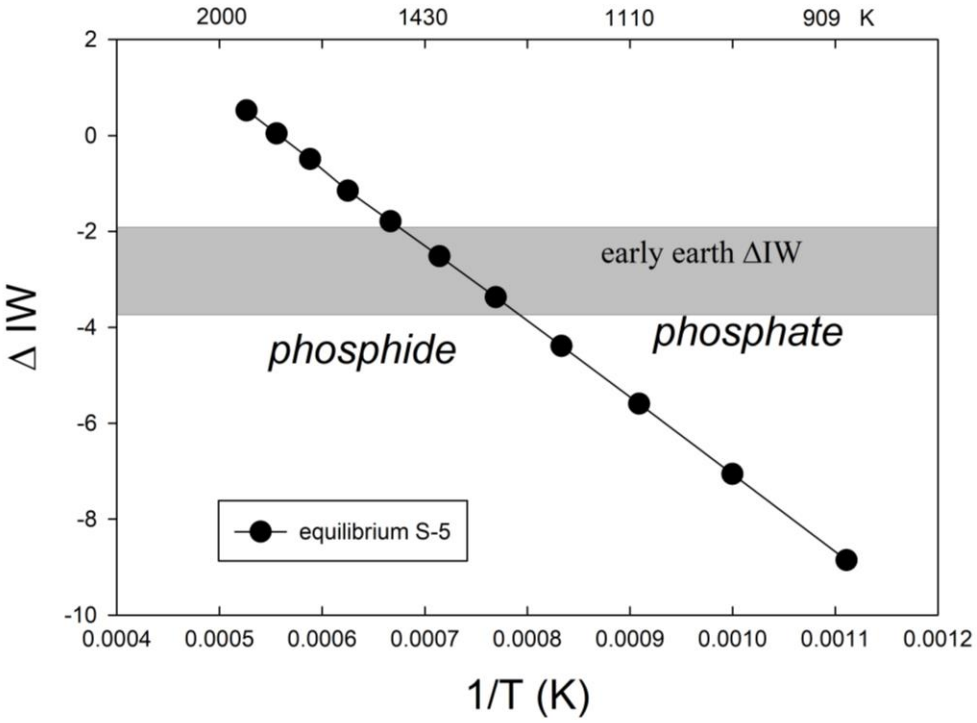

Figure S-3 Oxygen fugacity relative to the iron-wüstite buffer (IW) calculated form thermodynamic data from Robie *et al*. (1978) for equilibrium (Eq. S-5). IW reference buffer is calculated using the expression of Campbell *et al*. (2009). Note that phosphide is stable at high temperatures and fO_2 of the early Earth. Calculations assume $aSiO_2 = aCaSiO_3 = aCa_3(PO_4)_2 = 1$, and aP = 0.01.

Supplementary Information References

Campbell, A.J., Danielson, L., Righter, K., Seagle, C.T., Wang, Y., Prakapenka, V.B. (2009) High pressure effects on the iron–iron oxide and nickel–nickel oxide oxygen fugacity buffers. *Earth and Planetary Science Letters* 286, 556-564.

Ertel, W., Dingwell, D.B., Sylvester, P. (2008) Siderophile elements in silicate melts—A review of the mechanically assisted equilibration technique and the nanonugget issue. *Chemical Geology* 248, 119-139.

Gaboardi, M., Humayun, M. (2009) Elemental fractionation during LA-ICP-MS analysis of silicate glasses: Implications for matrix-independent standardization. *Journal of Analytical Atomic Spectrometry* 24, 1188-1197.

Holzheid, A., Palme, H., Chakraborty, S. (1997) The activities of NiO, CoO and FeO in silicate melts. *Chemical Geology* 139, 21-38.

Humayun, M., Simon, S.B., Grossman, L. (2007) Tungsten and hafnium distribution in calcium–aluminum inclusions (CAIs) from Allende and Efremovka. *Geochimica et Cosmochimica Acta* 71, 4609-4627.

Humayun, M. (2012) Chondrule cooling rates inferred from diffusive profiles in metal lumps from the Acfer 097 CR2 chondrite. *Meteoritics & Planetary Science* 47, 1191-1208.

Jochum, K.P., Weis, U., Stoll, B., Kuzmin, D., Yang, Q., Raczek, I., Günther, D. (2011) Determination of reference values for NIST SRM 610–617 glasses following ISO guidelines. *Geostandards and Geoanalytical Research* 35, 397-429.

Leinenweber, K.D., Tyburczy, J.A., Sharp, T.G., Soignard, E., Diedrich, T., Petuskey, W.B., Wang, Y., Mosenfelder, J.L. (2012) Cell assemblies for reproducible multi-anvil experiments (the COMPRES assemblies). *American Mineralogist* 97, 353–368.

Lewis, R.D., Lofgren, G.E., Franzen, H.F., Windom, K.E. (1993) The effect of Na vapor on the Na content of chondrules. *Meteoritics* 28, 622–628.

Lupis, C.H. (1983) Chemical Thermodynamics of Materials. Elsevier Science Publishing Co., Inc., New York, NY., 581 pp.

Ma, Z. (2001) Thermodynamic description for concentrated metallic solutions using interaction parameters. *Metallurgical and Materials Transactions B* 32, 87-103.

Malavergne, V., Charon, E., Jones, J., Cordier, P., Righter, K., Deldicque, D., Hennet, L. (2016) The formation of nuggets of highly siderophile elements in quenched silicate melts at high temperatures: Before or during the silicate quench? *Earth and Planetary Science Letters* 434, 197-207.

Pasek, M.A. (2008) Rethinking early Earth phosphorus geochemistry. *Proceedings of the National Academy of Sciences* 105, 853-858.

Righter, K., Humayun, M., Danielson, L. (2008) Partitioning of palladium at high pressures and temperatures during core formation. *Nature Geoscience* 1, 321-323.

Righter, K., Danielson, L.R., Pando, K., Williams, J., Humayun, M., Hervig, R.L., Sharp, T.G. (2015) Mantle HSE abundances in Mars due to core formation at high pressure and temperature. *Meteoritics & Planetary Science* 50, 604-631.

Righter, K., Nickodem, K., Pando, K., Danielson, L., Boujibar, A., Righter, M., Lapen, T.J. (2017) Distribution of Sb, As, Ge, and In between metal and silicate during accretion and core formation in the Earth. *Geochimica et Cosmochimica Acta* 198, 1-16.

Righter, K., Pando, K., Humayun, M., Waeselmann, N., Yang, S., Boujibar, A., Danielson, L.R. (2018) Effect of silicon on activity coefficients of siderophile elements (Au, Pd, Pt, P, Ga, Cu, Zn, and Pb) in liquid Fe: Roles of core formation, late sulfide matte, and late veneer in shaping terrestrial mantle geochemistry. *Geochimica et Cosmochimica Acta* 232, 101-123.

Robie, R.A., Hemingway, B.S., Fisher, J.R. (1978) Thermodynamic properties of minerals and related substances at 298.15 K and 1 Bar (10^5 Pascals) pressure and at higher temperatures. *United States Geological Survey Bulletin* 1452, Washington DC, 461 pp.

Walker, D., Carpenter, M.A., Hitch, C.M. (1990) Some simplifications to multianvil devices for high pressure experiments. *American Mineralogist* 75, 1020-1028.

Walker, R.J., McDonough, W.F., Honesto, J., Chabot, N.L., McCoy, T.J., Ash, R.D., Bellucci, J.J. (2008) Modeling fractional crystallization of group IVB iron meteorites. *Geochimica et Cosmochimica Acta* 72, 2198-2216.

Wasson, J.T., Ouyang, X., Wang, J., Jerde, E. (1989) Chemical classification of iron meteorites: XI. Multi-element studies of 38 new irons and the high abundance of ungrouped irons from Antarctica. *Geochimica et Cosmochimica Acta* 53, 735-744.

Wood, B.J., Kiseeva, E.S., Mirolo, F.J. (2014) Accretion and core formation: The effects of sulfur on metal–silicate partition coefficients. *Geochimica et Cosmochimica Acta* 145, 248-267.

Yang, S., Humayun, M., Righter, K., Jefferson, G., Fields, D., Irving, A.J. (2015) Siderophile and chalcophile element abundances in shergottites: Implications for Martian core formation. *Meteoritics & Planetary Science* 50, 691-714.